

Review

Prussian Blue and Its Analogs as Novel Nanostructured Antibacterial Materials

Angelo Taglietti ¹ , Piersandro Pallavicini ¹  and Giacomo Dacarro ^{1,2,*} 

¹ Dipartimento di Chimica, Università degli Studi di Pavia, Via Taramelli 12, I-27100 Pavia, Italy; angelo.taglietti@unipv.it (A.T.); piersandro.pallavicini@unipv.it (P.P.)

² CHT, Centre for Health Technologies, Università degli Studi di Pavia, Via Taramelli 12, I-27100 Pavia, Italy

* Correspondence: giacomo.dacarro@unipv.it; Tel.: +39-382-987-337

Abstract: Prussian blue is an ancient artificial pigment. Its biocompatibility and the possibility of synthesizing it in nanometric size stimulated the interest of the scientific community. Many uses of Prussian blue nanoparticles have been reported in the field of nanomedicine. More recently, interest into the potential application of Prussian blue nanoparticles as antibacterial agents has spread. Literature regarding Prussian blue and its analogs as antibacterial materials is still limited, but the number of papers has grown quickly over the last 2–3 years.

Keywords: Prussian blue; nanoparticle; antibacterial; photothermal; nanomaterial



Citation: Taglietti, A.; Pallavicini, P.; Dacarro, G. Prussian Blue and Its Analogs as Novel Nanostructured Antibacterial Materials. *Appl. Nano* **2021**, *2*, 85–97. <https://doi.org/10.3390/applnano2020008>

Academic Editor: Dimitrios Bikiaris

Received: 17 March 2021

Accepted: 23 April 2021

Published: 28 April 2021

Publisher's Note: MDPI stays neutral with regard to jurisdictional claims in published maps and institutional affiliations.



Copyright: © 2021 by the authors. Licensee MDPI, Basel, Switzerland. This article is an open access article distributed under the terms and conditions of the Creative Commons Attribution (CC BY) license (<https://creativecommons.org/licenses/by/4.0/>).

1. Introduction

Prussian blue (PB) is considered the first synthetic coordination compound, as well as the first purely synthetic pigment. The first mention of PB in literature dates back to 1710, in a publication of the Royal Prussian Society of Sciences entitled “The miscellanea Berolinensia ad incrementum Scientiarum” [1]. The manuscript, however, is vague on the discovery of the pigment. The most credited version of the story says that PB was discovered by a German (Prussian) color-maker named Diesbach, who was actually trying to prepare a red pigment: Florentin lake [2]. Due to a contamination of the potash (potassium carbonate) he used, the obtained pigment came out blue and was named Berlin blue or, more commonly, Prussian blue, after the home country of Diesbach. Due to its low cost and ease of preparation, PB quickly overcame other blue pigments like ultramarine.

When the composition of PB became more clear, it was identified as a complex iron cyanide, with cyanide ligands bridging Fe(II) and Fe(III) ions. The classical preparation of PB involves a simple mixing of aqueous Fe(III) and $[\text{Fe}(\text{CN})_6]^{4-}$. An alternative preparation, made by mixing Fe(II) salts with $[\text{Fe}(\text{CN})_6]^{3-}$, was, for a long time, identified as Turnbull's blue and believed to be a different product. Instrumental structural analysis, however, proved that Prussian blue and Turnbull's blue are exactly the same product [3]; see, for example, the X-ray structure of PB and similar products reported in 1936 by Keggin and Miles [4].

The first model for the electron transition responsible for the blue color was proposed in 1962 by Robin, using the ligand field theory [5]: although the starting materials have very different spectra, the intense blue absorption in PB is due to an intervalence band, i.e., a charge transfer transition between $[\text{Fe}(\text{CN})_6]^{4-}$ and Fe(III) ions.

Besides being known for such a long time, uncertainties on the structure and properties of PB remained for several decades, and only recently have all of the doubts been solved [6]. The mixing of Fe(III) salts and potassium hexacyanoferrate, $\text{K}_4[\text{Fe}(\text{CN})_6]$, can indeed lead to the formation of products with different formulas. PB is conventionally labeled as “soluble”, with the formula $\text{KFe}^{\text{III}}[\text{Fe}^{\text{II}}(\text{CN})_6] \cdot x\text{H}_2\text{O}$ ($x = 1\text{--}5$), and “insoluble”, $\text{Fe}^{\text{III}}_4[\text{Fe}^{\text{II}}(\text{CN})_6]_3 \cdot x\text{H}_2\text{O}$ ($x = 14\text{--}16$). The two formulas, however, define the same product, the different solubility being related only to the different crystal size. Detailed diffraction

studies showed that, in all its crystalline forms, PB has a face-centered cubic lattice with alternate Fe(II) and Fe(III) ions bridged by cyanide anions. In the soluble form (Figure 1a), [7] K^+ is present in the center of half of the cubic cells. In the “insoluble” PB, on the other hand, $[Fe(CN)_6]^{4-}$ anions are substoichiometric, leaving one quarter of the Fe(III) coordinatively unsaturated. In this form of PB, the free positions on Fe(III) are occupied by water molecules (Figure 1a).

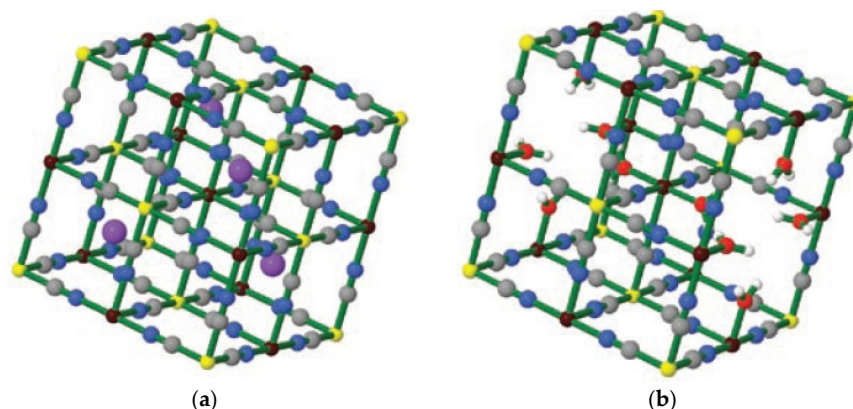


Figure 1. (a) Rendering of the lattice of ‘soluble’ PB, $KFe^{III}[Fe^{II}(CN)_6]$, with half of the centers of the cubic cells occupied by K^+ . Colors: Fe^{II} yellow, Fe^{III} brown, C gray, N blue, K violet; (b) Rendering of the lattice of ‘insoluble’ PB, $Fe^{III}_4[Fe^{II}(CN)_6]_3$, with the coordinative sphere of Fe^{III} completed by water molecules (O red, H white). Reprinted with permission from ref. [7]. Copyright 2008 American Chemical Society.

As we mentioned before, PB was traditionally divided into “soluble” and “insoluble” preparations. The two preparations, however, are both of insoluble products, strictly speaking. The difference between the two is simply in the size of particles: depending on synthetic parameters, in fact, PB can precipitate in bulk or nanometric crystals. In the second case, a stable colloid (that was inappropriately considered a solution) can be obtained. Although PB colloids are reported in literature since the beginning of the 20th century [8], papers reporting synthesis with controlled size and shape of the particles were published only in the last two decades [9], giving rise to a growing interest for PB nanomaterials in several fields. In 2003, the FDA approved the use of PB for treatment of radiation contamination due to cesium or thallium [10]. In particular Radiogardase[®], a product made of insoluble PB capsules, was approved for the removal of harmful levels of cesium-137 and thallium.

Its ease of synthesis in nanometric form [10,11] and its certified biocompatibility [12–15] made PB an ideal candidate for the preparation of nanomaterials of medical and biomedical interest. This gave rise to great interest from the academic community and to a high number of publications dedicated to PB. In the last three years, around 20 reviews per year were published on the topic “Prussian blue”. Recently, the biomedical applications of PB have been reviewed in depth [16]. PB in nanomedicine is used for imaging [17], drug delivery [18], photothermal therapy [19] and, as mentioned before, the classical application as an antidote for Cs and Tl poisoning.

In 2017, a review was also dedicated to Prussian blue analogs (PBA) [20], i.e., all those compounds with formula $A_xM_y[M'(CN)_6]_z$, where A is an alkaline metal cation, and M and M' are metal cations in oxidation state +2 or +3. The possibility of changing, partially or entirely, one Fe ion or both offers interesting possibilities for the biomedical use of these coordination polymers. The introduction of Gd^{III} [21] and Mn^{II} [22] ions improves the performance of PB as a T1 contrast agent in magnetic resonance imaging (MRI). Through further doping with a lanthanide ion, multimodal imaging with combined MRI and fluorescence is possible [23]. The same effect can be achieved by coating PBA nanoparticles with a fluorophore-containing polymer [24]. Regarding therapy, PBA's absorption band

can be completely shifted with respect to pure PB, lacking a good positioning of the band in the biotransparent window. A limited doping of a non-Fe metal (e.g., Mn^{II}), however, can induce a red-shift in the band of PB, improving its photothermal activity [22].

Among the many fields of application of Prussian blue and its analogs, we must also cite the electrochemical properties, which can be exploited in the field of biosensing. This aspect has been reviewed in detail by Karyakin in 2017 [25] and by Matos-Peralta and Antuch in 2019 [26].

It might seem that all the aspects of PBNP preparation and its potential applications are already extensively discussed in literature, but recently several papers started to appear exploring a new possibility in the use of PBNPs and their analogs: many of these nanomaterials show an antibacterial effect, both intrinsic to the material or switchable, exploiting the photothermal effect. Though the number of papers on this topic is still limited, we noticed a quick increase in their number over the last year, and we think that this short review could be a useful starting point for upcoming studies. We will summarize the papers that already reported the antibacterial effects of PB and PBA and give an overview of different approaches to the preparation and application of those nanomaterials.

2. Synthesis and Coating

PBNP synthesis has been thoroughly described elsewhere and is not the main focus of this review. We will however go through the main synthetic pathways for this nanomaterial.

As we reported in the introduction, PB has been known since the early 18th century and was traditionally divided into “soluble” and “insoluble” forms. The former referred to a more dispersible, nanosized particulate, rather than to an actually soluble product.

At present, many synthetic routes have been explored for the preparation of PBNPs. Synthesis can be carried out in water or in solvent, the first being more attractive due to the lower cost, green conditions and ease of application in biology and medicine. Aqueous synthesis, on the other hand, usually offers less control on the size and shape of the nanoparticles. Several approaches are used for the preparation of PB and PBAs, such as microemulsions [27] and sonochemical, hydrothermal and microwave-assisted syntheses [28], but the most-used approach is coprecipitation synthesis, based on the mixing of two Fe salts in different oxidation states (i.e., Fe^{II} and Fe^{III}), in the presence or absence of a stabilizing agent. A good overview of this synthetic method can be found in the papers from Grandjean, Samain et al. [16,29], who also examined “indirect” synthesis, involving firstly, the coprecipitation of Fe^{II} salts, leading to the formation of so-called Prussian white and a subsequent oxidation to Prussian blue. The authors also cite two different options in the choice of iron salts: Fe^{III} and $[\text{Fe}^{\text{II}}(\text{CN})_6]^{4-}$ or Fe^{II} and $[\text{Fe}^{\text{III}}(\text{CN})_6]^{3-}$: as we mentioned before, the two routes were historically considered different syntheses (Prussian blue vs. Turnbull’s blue), but this distinction is nowadays meaningless, as they lead to the same product. An alternative method of synthesis is the use of a single precursor (i.e., an Fe^{II} or Fe^{III}) source, followed by a slow and controlled reduction-/oxidation-generating iron in the other oxidation state [30,31].

The first reports of a rationalized synthesis of nanometric PB date around the year 2000. Vaucher and coworkers [9] published a synthesis based on AOT reverse microemulsion in isoctane. The photochemical synthesis exploited a slow photoreduction of $[\text{Fe}^{\text{III}}(\text{C}_2\text{O}_4)_3]^{2-}$ into Fe^{2+} in the presence of $[\text{Fe}^{\text{III}}(\text{CN})_6]^{3-}$ ions, leading to cubic nanoparticles with an average size of 12–16 nm.

The size tuning of PBNPs was achieved in 2003 by Uemura et al. [11], through a synthesis based on the mixing of Fe^{2+} and $[\text{Fe}^{\text{III}}(\text{CN})_6]^{3-}$ in water, yielding spherical particles between 12 and 25 nm in size. Size tuning was achieved with different concentrations of Fe ions. A PVP coating grants stability to the colloids and allows the isolation of the product in solid form. The amphiphilic properties of the polymer also allow the redispersion of the PBNPs in different solvents. PVP-assisted synthesis also allows also the production of ultrasmall PBNPs, with a size of 3.4 nm [32], and grants very good control over the cubic shape of the particles. As Gu and colleagues pointed out in a recent review [33], many

other polymers can be used as stabilizing agents in the synthesis of PBNPs, leading to tunable surface properties of the nanomaterials.

3. Antibacterial Activity of Prussian Blue

3.1. Photothermal Antibacterial Effect of Prussian Blue Nanoparticles

The potential antibacterial and antibiofilm activity of Prussian blue has been evaluated only in recent years. The composition of this coordination polymer does not suggest the presence of an intrinsic activity, since iron salts are not known to have any (in contrast, for example, to well-known antibacterial metals like silver and copper, which also maintain their activity in nanometric form). The absence of an intrinsic antibacterial effect was confirmed by a report from Somani et al. in 2013 [34]. In this study, the authors simply tested the activity of Prussian blue on four different bacterial strains (*Salmonella typhi*, *Staphylococcus aureus*, *Pseudomonas aeruginosa* and *Shigella*). Few details were reported on the type of PB used: presumably insoluble and not nanostructured, according to the formula reported in the paper and the insolubility in water reported by the producer. Antibacterial activity tests, performed with the agar diffusion and dilution methods, gave negative results on all the strains. After this first rough report, the potential of PB as an antibacterial material was completely neglected until 2016. Larionova and colleagues do not mention antibacterial activity in their paper, “Prussian Blue nanoparticles for biomedical applications”: PB is proposed as a medium for drug delivery, therapy, multifunctional nanoprobe, imaging and the well-known application as an antidote for Cs and Tl poisoning. In therapeutic application, a lot of attention is given to the photothermal effect. This effect was proven against bacteria for metal nanoparticles, e.g., gold [35,36] and silver [37].

Following the same approach (i.e., exploiting a photothermal effect to kill bacteria) Boukherroub et al. tested PVP-coated PBNPs against antibiotic-resistant Gram-positive and Gram-negative bacteria. The authors tested the photothermal effect of PBNPs at two different wavelengths in the near infrared (NIR): 810 nm and 980 nm. The maximum absorption wavelength is, as usual for PB, around 700 nm, but the use of higher irradiation wavelengths allows operation in the biotransparent window, a crucial requisite if the material is used in vivo. The temperature increase is proportional to the concentration of nanoparticles and is higher when the irradiation wavelength is 810 nm (with respect to 980 nm). This is perfectly compatible with the data we acquired on a similar material (i.e., citrate-coated PBNPs): the photothermal effect is proportional to absorbance at the irradiation wavelength, as we verified with four different lasers (730, 800, 940 and 1064 nm) [38]. Moreover, we also verified that the magnitude of the photothermal effect is proportional to the employed laser power. In a 20–100 mW interval (laser beam waist was 2.6 mm), ΔT increases linearly with laser power (see Figure 2).

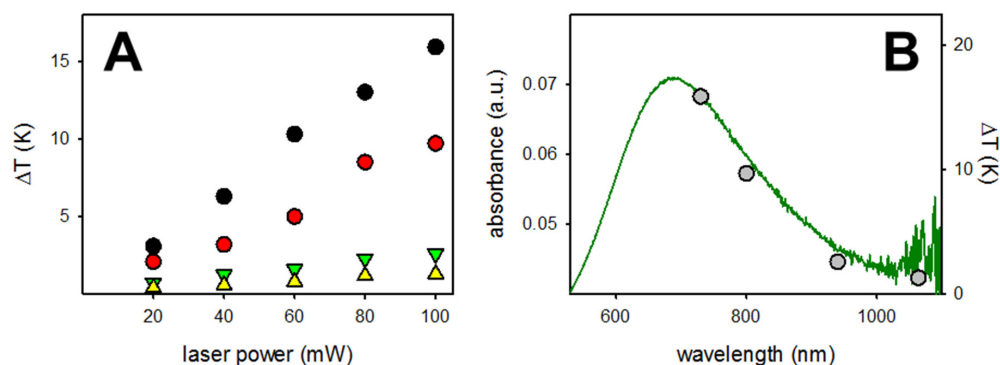


Figure 2. Photothermal effect on a PBNP monolayer (reproduced with permission from ref. [39], copyright Taylor and Francis 2017): (A) Photothermal effect vs. laser power at different wavelengths: black circles–730 nm, red circles–800 nm, green triangles–940 nm, yellow triangles–1064 nm; (B) ΔT values found for the four wavelengths used for irradiation at 100 mW power, superimposed to the UV–Vis absorption spectrum.

Boukherroub tested the photothermal antibacterial effect of PVP-coated PBNPs with 10 min of laser irradiation at a 1 W/cm^2 irradiance. Good results were reported against both Gram-positive and Gram-negative bacteria: extended spectrum β -lactamase (ESBL) *E. coli* and methicillin-resistant *Staphylococcus aureus* (MRSA). Viable bacterial cells were reduced by 5–6 orders of magnitude with PBNP concentrations lower than $100 \mu\text{g/mL}$. The authors also suggest that, at a proper concentration ($<50 \mu\text{g mL}^{-1}$) and wavelength (980 nm), the antibacterial effect can be selectively exerted over cytotoxicity on mammalian cells.

Lower effects are recorded when PBNPs are anchored on self-assembled monolayers, as we reported in 2017 [38]: in this case nanoparticle concentration is lower (0.38 mg/cm^2 , expressed as Fe concentration), and we employed a low irradiance, 0.25 W/cm^2 , in order to respect the recommended limits for tissue irradiation. We reported that, in these conditions, microbicidal effect is higher against Gram-negative bacteria (*E. coli*) than against Gram-positive strains (*S. aureus*). This coheres with what we found for similar nanoparticle-functionalized surfaces: Gram-positive bacteria always show higher resistance [39].

PBNP were also employed by Borzenkov and us in the formation of PVA hydrogels [40] and sprayed films [41]. PVA was chosen for its biocompatibility and ease of preparation as a film, making it an ideal material for medical devices and food packaging. PB-loaded PVA films were tested for their photothermal effect, confirming that a high hyperthermia is also achieved in this material, and their activity was tested against *P. aeruginosa*, a biofilm-forming Gram- bacteria. The photothermal effect was measured with irradiation at 700 nm and 800 nm, the former leading to a higher temperature increase, the latter being more suitable for in vivo use. The temperature increase, as previously demonstrated for colloids and monolayers, is proportional to the laser irradiance.

PB-loaded PVA films and sprayed films were tested against planktonic bacteria and biofilms, showing a good activity in both cases. The antibacterial effect was evaluated with confocal microscopy, obtaining a quantitative evaluation (expressed as the ratio of dead/alive cells) and qualitative imaging, as shown in Figure 3 for the antibiofilm activity. The sprayed films of PVA also show a good activity against Gram+ bacteria (*S. aureus*).

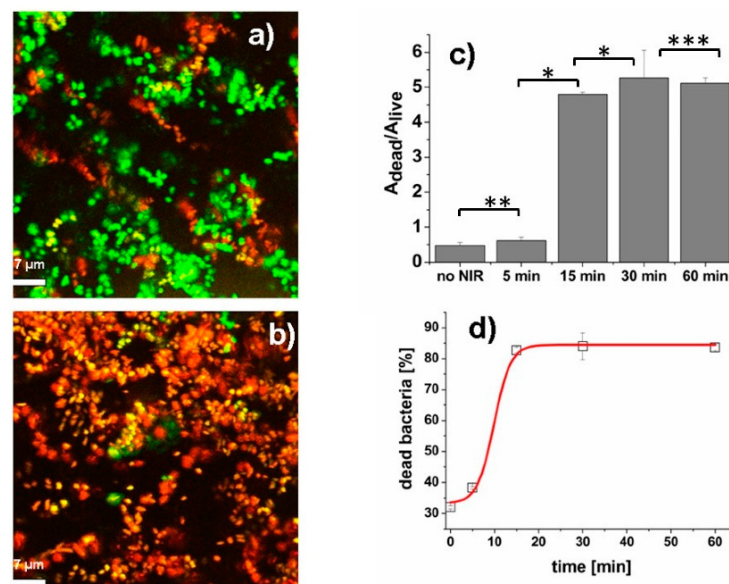


Figure 3. Antibiofilm effect of a sprayed PB-containing film, reproduced from ref. [42]: (a) confocal image of *P. aeruginosa* bacteria on sprayed film without NIR irradiation; (b) confocal image of bacteria on sprayed film after 15 min of NIR irradiation; (c) the dependence of ratio $A_{\text{dead}}/A_{\text{live}}$ as a function of NIR-exposure duration; (d) the dependence of dead bacteria fraction (%) as a function of NIR irradiation duration. Data are best fit to a sigmoidal function (red line). The symbols *, **, *** indicate that the two samples t-Test provides $p < 0.001$, $p = 0.009$ and $p = 0.43$, respectively.

All of these papers are oriented towards in vivo applications and to the functionalization of biomedical devices. Yu and colleagues proposed another field of applications for PBNPs, which could have great potential: photothermal sterilization of water [42]. In this case, Prussian blue nanocages were used instead of solid nanoparticles. The optical properties of nanocages were not different, with the usual absorption band centered around 700 nm, but hollow nanoparticles showed a higher photothermal conversion efficiency when compared to solid PBNPs. The photothermal effect was verified with NIR laser irradiation at 808 nm (2 W/cm^2 irradiance) and with mild solar light irradiation. The temperature increase, as expected, is concentration- and irradiation-time-dependent and can be exploited for the thermal inactivation of bacteria. *E. coli* colonies were successfully inactivated with 5 min of irradiation and a concentration of PB nanocages of $100 \mu\text{g/mL}$, and promising results were also reported for a sample of contaminated water containing multiple strains of bacteria. Irradiation for 10 min at a $100 \mu\text{g/mL}$ concentration of PB nanocages led to a killing rate near 100% on a contaminated tap water sample.

The same authors also published a paper on PB-encapsulated Fe_3O_4 nanoparticles, designed for the same purpose, i.e., the decontamination of water [43]. In this paper, the photothermal inactivation of bacteria was tested against Gram+ (*S. aureus*) and Gram- (*E. coli*) bacteria, in addition to contaminated water samples. The photothermal efficiency of this core-shell material is intermediate between the two components: iron oxide and Prussian blue, but is still sufficient to reach temperatures above $50 \text{ }^\circ\text{C}$ with solar light irradiation. The presence of a magnetic material (i.e., Fe_3O_4) makes the material reusable: the authors demonstrated that the nanoparticles can be effectively separated from water just by applying an external magnetic field. The photothermal disinfection capability of the material remains unchanged after several cycles.

PBNPs also offer the possibility of combining the effect of the inorganic material with a functional organic coating. Hua and colleagues studied the effect of acetylcysteine-coated PBNPs in vitro and in vivo against bacteria responsible for focal infections [44]. Acetylcysteine is used as a capping agent during synthesis (in substitution of usual capping agents as citrate or PVP), exploiting the strong bond formed between sulfur and iron atoms. Acetylcysteine is a mucolytic agent and an antibacterial with low toxicity. The authors expected a synergic effect with the photothermal activity of PBNPs, in order to kill planktonic bacterial cells and reduce the formation of biofilms and abscesses, which are usually associated with the formation of mucus. An acetylcysteine coating increases the biocompatibility of PBNPs, as tested with human dermal fibroblasts (HDF), using PVP-coated PBNPs as comparison. On the other hand, an increase in the intrinsic antibacterial effect was reported, again comparing AC-PBNP and PVP-PBNP. The photothermal antibacterial effect is high in both PVP and acetylcysteine-coated PB, the latter being less cytotoxic, as mentioned before. The antibacterial effect was tested against *S. aureus* and *E. coli*, with good results against both strains: survival rates of 3% were measured with 10 min of irradiation.

The most interesting result in this paper is represented by the in vivo tests: subcutaneous *S. aureus* infections in mice were treated with PB, acetylcysteine-coated PB and NIR irradiation (980 nm , 2 W/cm^2), with untreated mice as a control group. Focal infections were caused by subcutaneous injection of *S. aureus* in Balb/c mice. The injection of AC-PB in the site reduced the formation of scabs, and this effect was ascribed by the authors to the antibacterial effect of nanoparticles. The combined effect of AC-PB injection and NIR irradiation led to significant wound repair, as evaluated by visual examination of the infection site and confirmed by histological examination: while a large number of inflammatory cells was detected in untreated infected mice, this was significantly reduced in the group treated with AC-PB and NIR irradiation.

The potential of PBNPs in the preparation of wound-healing materials was also reported in a recent paper from Wu et al. [45]. PBNPs were included in a chitosan hydrogel, in order to combine the photothermal properties of Prussian blue with the well-known biocompatibility and hydrogel-forming properties of chitosan (along with the weak intrinsic antibacterial effect of the polymer). PVP-coated PBNPs were entrapped in a hydrogel

made of a functionalized chitosan, bearing quaternary amines and double bonds, with antibacterial and crosslinking functions, respectively.

The authors claim that the electropositive surface of the gel is capable of attracting bacterial cells and can damage their membrane. This is confirmed by the intrinsic antibacterial effect of the chitosan hydrogel, which is not influenced by the presence of PB. When irradiation at 808 nm is present, however, the effect changes noticeably. A photothermal effect is added to the intrinsic effect, the former being dependent on the concentration of PBNPs present in the hydrogel. This allows an increase in the antibacterial activity “on demand” through laser irradiation. A killing rate of over 99.9% (compared to a $\approx 40\%$ of the hydrogel alone) was reported against *E. coli* and *S. aureus* with low irradiances (0.3 W/cm^2) but, on the other hand, hydrogels showed a low cytotoxicity against fibroblasts. PBNP-loaded hydrogels proved highly efficient also in tests in vivo: infection of wounds was limited in the presence of the photothermal material, and the wound-healing process was significantly faster. Infected wounds treated with PB-loaded hydrogels closed in shorter times than control groups treated with chitosan only and standard gauze. The results were also supported by histological tests showing no inflammation on the PB-treated mice four days after the infection, while all of the test groups still showed large numbers of inflammatory cells.

3.2. Prussian Blue Doped with Traditional Antibiotics

Usually inorganic nanomaterials are seen as an alternative to traditional organic antibiotics. A combination of the two, however, can activate a synergic effect or improve the performances of the two isolated materials, opening new possibilities in antibacterial treatment.

In this perspective, an interesting approach has been proposed by Liu and coworkers in two recent papers. PB nanoparticles [46] and Au@PB [47] core-shell nanostructures were decorated with vancomycin, a well-known antibiotic present in the WHO list of essential medicines. The binding of vancomycin on PBNP has a double function: it imparts an increased antibacterial and wound-healing effect when compared to bare PBNPs, and it can act as a targeting unit in the sensing of bacteria. The incubation of *S. aureus* with different concentrations of vancomycin-doped particles showed that the nanoparticles effectively bind to the bacteria, as shown by SEM imaging and photothermal measurements on isolated bacteria after incubation. Vancomycin-doped PBNPs and Au@PBNP core-shell structures were exploited for the sensing of Gram-positive bacteria (*S. aureus*) with different detection techniques: Raman sensing, pressure reading and temperature reading.

3.3. Prussian Blue Analogs with Antibacterial Effect

Prussian blue analogs (PBA) are a valid alternative to PB in many fields of applications. The complete or partial substitution of Fe^{II} , Fe^{III} or both leads to a plethora of interesting compounds. If we speak of photothermal compounds, however, the substitution of one or both of the iron ions unavoidably modifies the absorption band of the coordination polymer. This can be a drawback because it can hinder the possibility of irradiation in the NIR. A study of Mukherjee and Patra [48], for example, describes a core-shell material made of silver nanoparticles enclosed in a PBA shell. The PBA contains Ni^{II} and Fe^{III} ions. In this case, the PBA is not photothermally active in the NIR, having a maximum absorption wavelength at around 400 nm. The core-shell structure, however, aids the stability of the material and its biocompatibility. NiPB@AgNC showed high stability in a saline solution at physiological pH: this is an improvement with respect to bare AgNP, which is typically sensitive to high ionic strengths and to chlorides in particular. Cytotoxicity tests show an improvement as well: NiPB-enclosed silver nanoparticles have a lower cytotoxicity in vitro. The antibacterial activity of this material was measured in comparison to traditional antibiotics (penicillin and streptomycin) by means of growth inhibition and zone of inhibition studies. NiPB@AgNC also showed a doubled antibacterial effect when compared to bare silver nanoparticles, confirming the positive effect of the NiPB shell.

To our knowledge, the first report of a PBA with an actual intrinsic antibacterial effect is the communication published in 2018 by Kim and Huang [49]. The paper describes a Ca/Fe^{III}-based analog, prepared in nanometric form with a PVP coating. CaPB is internalized by bacterial cells and depletes intracellular iron through an ion-exchange reaction, leading to the formation of insoluble PB. This simple mechanism is highly effective and selective, leading to a three-fold reduction in Fe concentration in a few hours. CaPB was successfully internalized in *S. aureus* bacterial cells and exerted a moderate antibacterial effect. Bacterial growth is inhibited over a 9 h period, with a dose-dependent decrease of viable cells up to 0.8 logarithmic units.

PBA can also have photothermal properties, as in the case of Zn-doped PB reported by Wu and colleagues [50]. Doping of PB with a different metal ion can induce a red-shift of the absorption band, improving the photothermal efficiency of the material under NIR irradiation. A similar behavior was reported also for Mn-doped PB [21]. Zn-doping in PB leads to cubic particles of greater size, and most importantly, shifts the maximum absorption wavelength up to 740 nm, starting from the characteristic 700 nm absorption of pure PB. This leads to a remarkable increase in absorption at 808 nm, improving the photothermal conversion efficiency. The local hyperthermia triggered by laser irradiation also increases Zn ions' release, leading to a synergistic antibacterial effect: a short irradiation (15 min) generates an immediate effect due to hyperthermia but also triggers ions' release, increasing the long-term intrinsic effect even hours after the irradiation (Figure 4). ZnPB proved to be effective against *E. coli*, *S. aureus*, MRSA (methicillin-resistant *Staphylococcus aureus*) and MRSA biofilms.

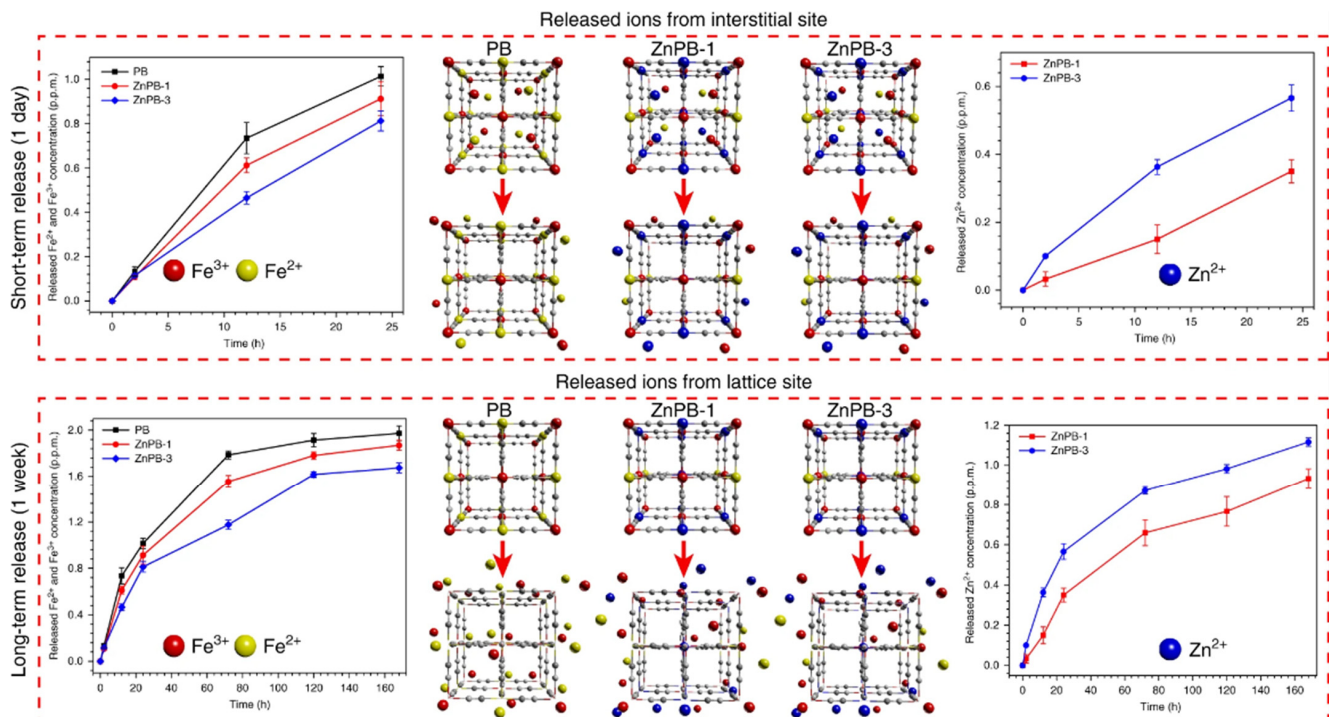


Figure 4. Zn-doped PB ions release behavior. Cumulative Fe²⁺, Fe³⁺ and Zn²⁺ release curves of PB, ZnPB–1 and ZnPB-3 (200 p.p.m.) at 37 °C in PBS for short-term release (one day) and long-term release (one week). Short-term released ions (one day) are mainly from the interstitial site and long-term released ions (one week) are mainly from the lattice site. Reproduced from ref. [51], Creative Commons Attribution 4.0.

Exploiting the balance between antibacterial effect and cytotoxicity, the authors also obtained good results with in vivo tests on MRSA wound infections. Wounds were exposed to a power density of 0.3 W/cm², a value within the scope of the maximum permissible exposure for skin formulated by the American National Standards Institute (ANSI Z136.1-

2000) in order to reach a temperature high enough to exert the antibacterial effect without damaging tissues and triggering inflammatory reactions. The results are remarkable in terms of antibacterial action and wound-closure speed, with improved performance when ZnPB is compared to traditional systemic and topical antibiotics (vancomycin, fusidic acid, retapamulin and mupirocin).

If d-block metals doping is the most obvious choice for the preparation of PBA (usually an ion of similar radius is chosen), lanthanides-doping also has interesting applications. Similarly to Zn, lanthanide ions also red-shift the maximum absorption wavelength [51]. Among the examined metal ions (Er^{3+} , Dy^{3+} , Tm^{3+} and Yb^{3+}), Yb^{3+} gave the best results. The maximum absorption wavelength shifts to 816 nm, and the photothermal conversion efficiency is increased from 46.6% (PB) to 55.0% (YbPB with 9% Fe replaced by Yb). A small increase was also reported in the photothermal antibacterial effect against *E. coli*.

3.4. Silver-Containing Prussian Blue

Silver, silver ions and nanosilver have been well known as antibacterial agents since ancient times. Surprisingly, to our knowledge, only three papers have been dedicated to silver-containing PB and PBAs. Each of the three reports a different approach: a silver Prussian blue analog without photothermal properties [52], a silver-doped PB with a photothermal effect [53] and PB nanoparticles decorated with silver nanoparticles [54].

The silver-PBA reported by Patra and colleagues [49] is prepared with the complete substitution of Fe^{II} ions with Ag^+ , leading to a coordination polymer with an absorption band centered at ≈ 400 nm, useless for potential irradiation in vivo. The material, however, showed promising intrinsic antibacterial effects against *E. coli*, *B. subtilis*, *K. pneumoniae* and *P. aeruginosa*, with performances comparable to traditional antibiotics, such as streptomycin, gentamicin, kanamycin and penicillin. The mechanism of action follows the typical mechanisms of silver: membrane damage, decreased expression of superoxide dismutase (SOD) and catalase and increased generation of lipid peroxidation.

With a similar approach, Roy et al. [50] prepared a silver-doped PB. The difference between the two syntheses are the choice of the stabilizer (citrate in this paper, PVP in Patra's paper) and the quantity of silver, which is here limited to 10% with respect to iron concentration. A partial substitution of Fe with a different metal ion, as we mentioned in the previous section, usually leads to a red-shift in the maximum absorption wavelength of PB. This is confirmed in the case of Ag-doped PB, with a maximum absorption wavelength red-shift of 31 nm. This allows the evaluation of both an intrinsic antibacterial effect and a photothermal effect with irradiation at 635 nm. The intrinsic effect against *S. aureus* and *P. aeruginosa* is comparable to what is reported for silver nanoparticles at the same concentration, while PB control samples, as expected, showed a negligible intrinsic effect. The triggering of the photothermal effect on Ag-doped PB led to a further increase in the effect, with almost complete elimination of the viable bacterial cells.

The third approach for PB/Ag hybrids is the decoration of PB nanoparticles with Ag nanoparticles. In the paper from Liu and coworkers [51], PBNP were coated with polydopamine (PDA). In a second functionalization step, Ag^+ is coordinated and reduced by PDA to form small spherical AgNP. PBNPs are around 90 nm in size, while AgNPs are less than 10 nm.

The presence of AgNPs does not influence the photothermal properties of PB, which, as usual, are dose- and power-dependent and can be exploited to exert a photothermal antibacterial effect. On the other hand, the presence of silver adds an intrinsic antibacterial effect to the nanomaterial, as demonstrated with an inhibition zone (without irradiation) test with *E. coli*, ampicillin-resistant *E. coli*, *S. aureus* and MRSA. Only the combination of the two effects, however, leads to a complete elimination of bacteria (>99% killed cells): this happens when the Ag/PBNP hybrid material is irradiated with NIR light (808 nm).

A study on the mechanism of action showed higher levels of ROS and higher oxidation of glutathione due to the release of Ag^+ . These effects are typical of silver-based materials and are accelerated by irradiation, thanks to the synergy with PB. All of the photothermal

materials (PB, PDA-coated PB and the hybrid Ag/PB material) also show an effect on the production of ATP, and in this case, the effect is maximized when Ag and the photothermal effect work in synergy.

4. Conclusions

Prussian blue is an ancient pigment, which, in its nanometric form, has recently become popular in nanomedicine. PB is currently studied in many fields, such as cancer therapy, imaging, etc. Recently, PB has also generated interest in the field of antibacterial materials, with an increasing number of papers appearing in the last few years. In this review, we tried to give an overview of this literature, examining the different approaches that can be adopted. PB can be used as a photothermal antibacterial material, in analogy with what happens in photothermal therapy in cancer, exploiting its absorption band in the visible–NIR portion of the spectrum. An intrinsic antibacterial effect can also be present if PB is doped with antibacterial ions or doped/coated with functional organic molecules. The two effects can also operate in synergy in materials that can exert a prolonged intrinsic effect but can also be enhanced with the external trigger of NIR light irradiation. A systematic comparison on the efficiency of those nanomaterials is not easy, since the different assays used to evaluate the antibacterial and antibiofilm effects require different conditions and concentrations of active material. In general, the range of concentrations used in the studies cited in this review varies from 5 to 200 $\mu\text{g}/\text{mL}$ for suspension. Concentrations are even lower when we consider films and monolayers working at an interface. Typically, PB and its derivatives were tested against *E. coli* and *S. aureus* as representatives of Gram- and Gram+ bacteria, respectively, showing good performance against both. In some studies, antibiotic-resistant bacteria were also considered (e.g., ampicillin-resistant *E. coli* and MRSA), and no specific resistance against PBNPs was reported.

This versatility, and the fact that PB is a recognized biocompatible material, offers a lot of possibilities in the application of this kind of nanomaterials, as sketched in Figure 5. We believe that the recent literature cited in this review will have great diffusion in the next couple of years, increasing interest in this topic.

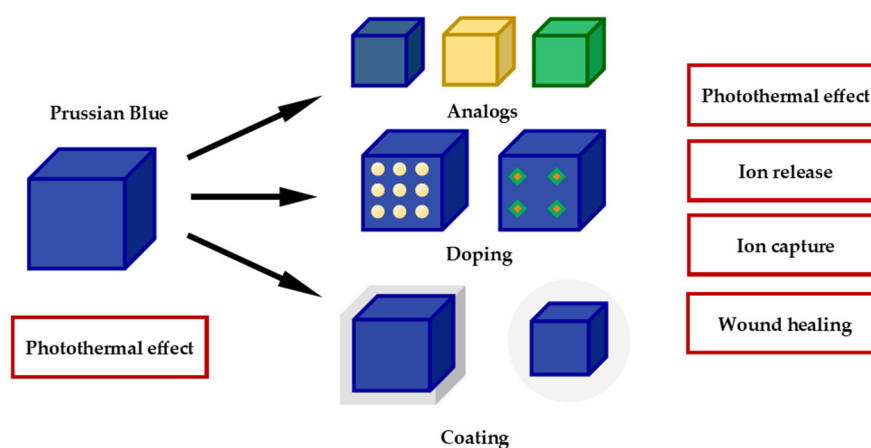


Figure 5. This pictorial sketch summarizes different approaches in the use of PB and its derivatives. While “plain” PB can be exploited only for its photothermal effect, the use of analogs, doped PB or coated/functionalized PB opens a plethora of possibilities, leading to one or more of the effect listed on the right.

Author Contributions: Writing and reviewing the manuscript (A.T., P.P., G.D.); All authors have read and agreed to the published version of the manuscript.

Funding: This research was funded by the Italian Ministero dell'Istruzione, dell'Università e della Ricerca, PRIN 2017 project 2017EKCS35.

Institutional Review Board Statement: Not applicable.

Informed Consent Statement: Not applicable.

Data Availability Statement: Not applicable.

Conflicts of Interest: The authors declare no conflict of interest.

References

1. Frisch, J.L. Notitia Caerulei Berolinensis Nuper Inventi. *Misc. Berolin. Incrementum Sci. Scr. Soc. Regiae Sci. Exhib. Ed.* **1710**, *1*, 777.
2. Kraft, A. On the discovery and history of Prussian blue. *Bull. Hyst. Chem.* **2008**, *33*, 61–67.
3. Ludi, A. Prussian Blue, an Inorganic Evergreen. *J. Chem. Edu.* **1981**, *58*, 1013. [CrossRef]
4. Keggin, J.F.; Miles, F.D. Structures and Formulae of the Prussian blues and Related Compounds. *Nature* **1936**, *137*, 577–578. [CrossRef]
5. Robin, M.B. The Color and Electronic Configurations of Prussian Blue. *Inorg. Chem.* **1962**, *1*, 337–342. [CrossRef]
6. Buser, H.J.; Schwarzenbach, D.; Petter, W.; Ludi, A. The Crystal Structure of Prussian Blue: $\text{Fe}_4[\text{Fe}(\text{CN})_6]_3 \cdot x\text{H}_2\text{O}$. *Inorg. Chem.* **1977**, *16*, 2704–2710. [CrossRef]
7. Ware, M. Prussian Blue: Artists' Pigment and Chemists' Sponge. *J. Chem. Educ.* **2008**, *85*, 612–621. [CrossRef]
8. Whitney, W.R.; Blake, J.C. On Colloidal Gold: Absorption Phenomena and Allotropy. *Am. J. Sci.* **1903**, *16*, 381–387. [CrossRef]
9. Vaucher, S.; Li, M.; Mann, S. Synthesis of Prussian Blue Nanoparticles and Nanocrystal Superlattices in Reverse Microemulsions. *Angew. Chem. Int. Ed.* **2000**, *39*, 1793–1796. [CrossRef]
10. Fda.Gov. Available online: <https://www.fda.gov/drugs/bioterrorism-and-drug-preparedness/fda-approves-first-new-drug-application-treatment-radiation-contamination-due-cesium-or-thallium> (accessed on 12 March 2021).
11. Uemura, T.; Kitagawa, S. Prussian Blue Nanoparticles Protected by Poly(vinylpyrrolidone). *J. Am. Chem. Soc.* **2003**, *125*, 7814–7815. [CrossRef] [PubMed]
12. Yang, Y.; Brownell, C.; Sadrieh, N.; May, J.; Del Grosso, A.; Place, D.; Leutzinger, E.; Duffy, E.; He, R.; Houn, F.; et al. Quantitative Measurement of Cyanide Released from Prussian Blue. *Clin. Toxicol.* **2007**, *45*, 776–781. [CrossRef]
13. Yang, Y.; Faustino, P.J.; Progar, J.J.; Brownell, C.R.; Sadrieh, N.; May, J.C.; Leutzinger, E.; Place, D.A.; Duffy, E.P.; Yu, L.X.; et al. Quantitative Determination of Thallium Binding to Ferric Hexacyanoferrate: Prussian Blue. *Int. J. Pharm.* **2008**, *353*, 187–194. [CrossRef]
14. Mohammad, A.; Faustino, P.J.; Khan, M.A.; Yang, Y. Long-Term Stability Study of Prussian Blue: A Quality Assessment of Water Content and Thallium Binding. *Int. J. Pharm.* **2014**, *477*, 122–127. [CrossRef]
15. Mohammad, A.; Yang, Y.; Khan, M.A.; Faustino, P.J. A Long-Term Stability Study of Prussian Blue: A Quality Assessment of Water Content and Cesium Binding. *J. Pharm. Biomed. Anal.* **2015**, *103*, 85–90. [CrossRef] [PubMed]
16. Long, J.; Guari, Y.; Larionova, J. Prussian Blue type nanoparticles for biomedical applications. *Dalton Trans.* **2016**, *45*, 17581. [CrossRef] [PubMed]
17. Gao, X.; Wang, Q.; Cheng, C.; Lin, S.; Lin, T.; Liu, C.; Han, X. The application of Prussian Blue nanoparticles in Tumor Diagnosis and Treatment. *Sensors* **2020**, *20*, 6905. [CrossRef] [PubMed]
18. Butler, J.S.; Sadler, P.J. Targeted delivery of platinum-based anticancer complexes. *Curr. Opin. Chem. Biol.* **2013**, *17*, 175–188. [CrossRef]
19. Dacarro, G.; Taglietti, A.; Pallavicini, P. Prussian Blue Nanoparticles as Versatile Photothermal Tools. *Molecules* **2018**, *23*, 1414. [CrossRef]
20. De Tacconi, N.R.; Rajeshwar, K. Metal Hexacyanoferrates: Electrosynthesis, in situ Characterization, and Applications. *Chem. Mater.* **2003**, *15*, 3046–3062. [CrossRef]
21. Kale, S.S.; Burga, R.A.; Sweeney, E.E.; Zun, Z.; Sze, R.W.; Tuesca, A.; Subramony, J.A.; Fernandes, R. Composite iron oxide–Prussian blue nanoparticles for magnetically guided T₁-weighted magnetic resonance imaging and photothermal therapy of tumors. *Int. J. Nanomed.* **2017**, *12*, 6413–6424. [CrossRef]
22. Zhu, W.; Liu, K.; Sun, X.; Wang, X.; Li, Y.; Cheng, L.; Liu, Z. Mn²⁺-Doped Prussian Blue Nanocubes for Bimodal Imaging and Photothermal Therapy with Enhanced Performance. *ACS Appl. Mater. Interfaces* **2015**, *7*, 11575–11582. [CrossRef] [PubMed]
23. Xu, M.; Chi, B.; Han, Z.; He, Y.; Tian, F.; Xu, Z.; Li, L.; Wang, J. Controllable synthesis of rare earth (Gd³⁺, Tm³⁺) doped Prussian blue for multimode imaging guided synergistic treatment. *Dalton Trans.* **2020**, *49*, 12327–12337. [CrossRef] [PubMed]
24. Forgach, L.; Hegedus, N.; Horvath, I.; Kiss, B.; Kovacs, N.; Varga, Z.; Jakab, G.; Kovacs, T.; Padmanabhan, P.; Szigeti, K.; et al. Fluorescent, Prussian Blue-Based Biocompatible Nanoparticle System for Multimodal Imaging Contrast. *Nanomaterials* **2020**, *10*, 1732. [CrossRef] [PubMed]
25. Karyakin, A.A. Advances of Prussian blue and its analogues in (bio)sensors. *Curr. Opin. Electrochem.* **2017**, *5*, 92–98. [CrossRef]

26. Matos-Peralta, Y.; Antuch, M. Prussian Blue and its analogs as appealing materials for electrochemical sensing and biosensing. *J. Electrochem. Soc.* **2020**, *167*, 037510. [[CrossRef](#)]
27. Bu, F.-X.; Du, C.-J.; Zhang, Q.-H.; Jiang, J.-S. One-pot synthesis of Prussian blue superparticles from reverse microemulsion. *CrystEngComm* **2014**, *16*, 3113–3120. [[CrossRef](#)]
28. Zakaria, M.B.; Chikyow, T. Recent advances in Prussian Blue analogues: Synthesis and thermal treatments. *Coord. Chem. Rev.* **2017**, *352*, 328–345. [[CrossRef](#)]
29. Samain, L.; Grandjean, F.; Long, G.J.; Martinetto, P.; Bordet, P.; Strivay, D. Relationship between the Synthesis of Prussian Blue Pigments, Their Color, Physical Properties, and Their Behavior in Paint Layers. *J. Phys. Chem. C* **2013**, *117*, 9693–9712. [[CrossRef](#)]
30. Karyakin, A.A.; Karyakina, E.E. Electroanalytical applications of Prussian Blue and its analogs. *Russ. Chem. Bull.* **2001**, *50*, 1811–1817. [[CrossRef](#)]
31. Jia, Z.; Sun, G. Preparation of Prussian Blue nanoparticles with single precursor. *Colloids Surf. A* **2007**, *302*, 326–329. [[CrossRef](#)]
32. Qin, Z.; Chen, B.; Mao, Y.; Shi, C.; Li, Y.; Huang, X.; Yang, F.; Gu, N. Achieving Ultrasmall Prussian Blue Nanoparticles as High-Performance Biomedical Agents with Multifunctions. *ACS Appl. Mater. Interfaces* **2020**, *12*, 57382–57390. [[CrossRef](#)]
33. Qin, Z.; Li, Y.; Gu, N. Progress in Applications of Prussian Blue Nanoparticles in Biomedicine. *Adv. Healthc. Mater.* **2018**, *7*, 1800347. [[CrossRef](#)]
34. Roy, A.K.; Somani, S.P.; Nene, A.; Bipinraj, N.K.; Somani, P.R. Antibacterial Activity of Prussian Blue. *J. Green Sci. Technol.* **2013**, *1*, 1–3. [[CrossRef](#)]
35. Pallavicini, P.; Donà, A.; Taglietti, A.; Minzioni, P.; Patrini, M.; Dacarro, G.; Chirico, G.; Sironi, L.; Bloise, N.; Visai, L.; et al. Self-assembled monolayers of gold nanostars: A convenient tool for near-IR photothermal biofilm eradication. *Chem. Commun.* **2014**, *50*, 1969–1971. [[CrossRef](#)] [[PubMed](#)]
36. Pallavicini, P.; Basile, S.; Chirico, G.; Dacarro, D.; D'Alfonso, L.; Donà, A.; Patrini, M.; Falqui, A.; Sironi, L.; Taglietti, A. Monolayers of gold nanostars with two near-IR LSPRs capable of additive photothermal response. *Chem. Commun.* **2015**, *51*, 12928–12930. [[CrossRef](#)]
37. D'Agostino, A.; Taglietti, A.; Grisoli, P.; Dacarro, G.; Cucca, L.; Patrini, M.; Pallavicini, P. Seed mediated growth of silver nanoplates on glass: Exploiting the bimodal antibacterial effect by near IR photo-thermal action and Ag⁺ release. *RSC Adv.* **2016**, *6*, 70414–70423. [[CrossRef](#)]
38. Dacarro, G.; Grisoli, P.; Borzenkov, M.; Milanese, C.; Fratini, E.; Ferraro, G.; Taglietti, A.; Pallavicini, P. Self-assembled monolayers of Prussian blue nanoparticles with photothermal effect. *Supramol. Chem.* **2017**, 823–833. [[CrossRef](#)]
39. Dacarro, G.; Cucca, L.; Grisoli, P.; Pallavicini, P.; Patrini, M.; Taglietti, A. Monolayers of polyethylenimine on flat glass: A versatile platform for cations coordination and nanoparticles grafting in the preparation of antibacterial surfaces. *Dalton Trans.* **2012**, *41*, 2456–2463. [[CrossRef](#)]
40. Borzenkov, M.; D'Alfonso, L.; Polissi, A.; Sperandeo, P.; Collini, M.; Dacarro, G.; Taglietti, A.; Chirico, G.; Pallavicini, P. Novel photo-thermally active polyvinyl alcohol-Prussian blue nanoparticles hydrogel films capable of eradicating bacteria and mitigating biofilms. *Nanotechnology* **2019**, *30*, 295702. [[CrossRef](#)] [[PubMed](#)]
41. Borzenkov, M.; Chirico, G.; Pallavicini, P.; Sperandeo, P.; Polissi, A.; Dacarro, G.; Doveri, L.; Collini, M.; Sironi, L.; Bouzin, M.; et al. Nanocomposite Sprayed Films with Photo-Thermal Properties for Remote Bacteria Eradication. *Nanomaterials* **2020**, *10*, 786. [[CrossRef](#)]
42. Jiang, T.; He, J.; Sun, L.; Wang, Y.; Li, Z.; Wang, Q.; Sun, Y.; Wang, W. Highly efficient photothermal sterilization of water mediated by Prussian blue nanocages. *Environ. Sci. Nano* **2018**, *5*, 1161. [[CrossRef](#)]
43. Jiang, T.; Wang, Y.; Li, Z.; Aslan, H.; Sun, L.; Sun, Y.; Wang, W.; Yu, M. Prussian blue-encapsulated Fe₃O₄ nanoparticles for reusable photothermal sterilization of water. *J. Coll. Int. Sci.* **2019**, *540*, 354–361. [[CrossRef](#)]
44. Cai, S.; Qian, J.; Yang, S.; Kuang, L.; Hu, D. Acetylcysteine-decorated Prussian blue nanoparticles for strong photothermal sterilization and focal infection treatment. *Colloids Surf. B* **2019**, *181*, 31–38. [[CrossRef](#)]
45. Han, D.; Li, Y.; Liu, X.; Li, B.; Han, Y.; Zheng, Y.; Wai, K.; Yeung, K.; Li, C.; Cui, Z.; et al. Rapid bacteria trapping and killing of metal-organic frameworks strengthened photo-responsive hydrogel for rapid tissue repair of bacterial infected wounds. *Chem. Eng. J.* **2020**, *396*, 125194. [[CrossRef](#)]
46. Hao, Z.; Lin, X.; Li, J.; Yin, Y.; Gao, X.; Wang, S.; Liu, Y. Multifunctional nanoplatfor for dual-mode sensitive detection of pathogenic bacteria and the real-time bacteria inactivation. *Biosens. Bioelectron.* **2021**, *173*, 112789. [[CrossRef](#)] [[PubMed](#)]
47. Gao, X.; Wu, H.; Hao, Z.; Ji, X.; Lin, X.; Wang, S.; Liu, Y. A multifunctional plasmonic chip for bacteria capture, imaging, detection, and in situ elimination for wound therapy. *Nanoscale* **2020**, *12*, 6489–6497. [[CrossRef](#)] [[PubMed](#)]
48. Mukherjee, S.; Das, S.; Nuthi, S.; Patra, C.R. Biocompatible nickel-prussian blue@silver nanocomposites show potent antibacterial activities. *Future Sci. OA* **2017**, *3*, FSO233. [[CrossRef](#)]
49. Wang, Z.; Yu, B.; Alamri, H.; Yarabarla, S.; Kim, M.-H.; Huang, S.D. KCa(H₂O)₂[Fe^{III}(CN)₆]-H₂O Nanoparticles as an Antimicrobial Agent against *Staphylococcus aureus*. *Angew. Chem. Int. Ed.* **2018**, *57*, 2214–2218. [[CrossRef](#)]
50. Li, J.; Liu, X.; Tan, L.; Cui, Z.; Yang, X.; Liang, Y.; Li, Z.; Zhu, S.; Zheng, Y.; Wai, K.; et al. Zinc-doped Prussian blue enhances photothermal clearance of *Staphylococcus aureus* and promotes tissue repair in infected wounds. *Nat. Commun.* **2019**, *10*, 4490. [[CrossRef](#)]
51. Chen, X.; Wua, G.; Tang, J.; Zhou, L.; Wei, S. Ytterbium-Doped Prussian blue: Fabrication, photothermal performance and antibacterial activity. *Inorg. Chem. Commun.* **2020**, *114*, 107821. [[CrossRef](#)]

-
52. Sharma, S.; Chakraborty, N.; Jha, D.; Gautam, H.K.; Roy, I. Robust dual modality antibacterial action using silver-Prussian blue nanoscale coordination polymer. *Mater. Sci. Eng. C* **2020**, *113*, 110982. [[CrossRef](#)] [[PubMed](#)]
 53. Mukherjee, S.; Kotcherlakota, R.; Haque, S.; Das, S.; Nuthi, S.; Bhattacharya, D.; Madhusudana, K.; Chakravarty, S.; Sistla, R.; Patra, C.R. Silver Prussian Blue Analogue Nanoparticles: Rationally Designed Advanced Nanomedicine for Multifunctional Biomedical Applications. *ACS Biomater. Sci. Eng.* **2020**, *6*, 690–704. [[CrossRef](#)] [[PubMed](#)]
 54. Tong, C.; Zhong, X.; Yang, Y.; Liu, X.; Zhong, G.; Xiao, C.; Liu, B.; Wang, W.; Yang, X. PB@PDA@Ag nanosystem for synergistically eradicating MRSA and accelerating diabetic wound healing assisted with laser irradiation. *Biomaterials* **2020**, *243*, 119936. [[CrossRef](#)] [[PubMed](#)]